scientific reports

Check for updates

OPEN

Optimization of catalytic wet oxidating fulvic acid with zero-valent copper chitosan activated carbon ball as the catalyst

Chaofei Song, Yue Lv, Xia Qin✉, Chengrui Guo, Jiaxin Cui & Wendkuuni Steve-Harold Kaghembega

The degradation efficiency of fulvic acid (FA) was investigated in the catalytic wet oxidation process (CWPO) by zero-valent copper chitosan activated carbon ball (ZVC/CTS-ACB). Characterization of ZVC/CTS-ACB shows that zero-valent copper was loaded successfully on the chitosan activated carbon. Plackett–Buiman (PB) design and response surface methodology (RSM) were employed to determine the influence factors and the optimum processing parameters. The model was well fitted to the actual data and the correlation coefficients of R^2 and R^2-adj were 0.9359 and 0.9039, respectively. Under the obtained optimum conditions for FA degradation: temperature = 94 °C and pH 3.8, the average FA removal by three replicate experiments was 93.02%, which has a high consistency to the RSM optimal target response of 93.86%. The comparison of catalytic performance showed that the addition of catalyst ZVC/CTS-ACS could increase the removal rate of FA, color number (CN) and TOC by 93.6%, 83.5% and 81.9% respectively. The high TOC removal rate indicated the good performance of the catalyst to FA mineralization. Additionally, the ICP analysis of copper ion leaching was only 0.08 mg/l after 5 repeated recycles of the catalyst, demonstrating the high stability of ZVC/CTS-ACB that is beneficial for the actual application.

Fulvic acid (FA), which is one major component of humic substances (HSs)[1–3], can be found in both natural waters and wastewater, especially in landfill leachate[1]. In the broadest terms, the structures of HSs can be described as assemblies of covalently linked aromatic and aliphatic residues carrying carboxyl, phenolic and alkoxy groups[2]. These common functional groups of FA make it possible that FA cause many serious environmental and health problems[3]. FA has strong complexation ability with heavy metals, leading to the formation of organometallic complexes with increased transportation ability, bioavailability and toxicity[4]. In the chlorination stage of the water treatment, FA and chlorine may produce a by-product trihalomethane whose strong carcinogenic and mutagenic properties seriously endanger human health[5–7]. Due to the complex structure, FA is frequently identified as refractory organic matter[8]. Therefore, biological methods are ineffective for FA treatment and many physical, chemical and physico-chemical methods have been employed for FA removal[9]. The advantages and disadvantages of these methods are summarized in Table 1.

Catalytic Wet Hydrogen Peroxide Oxidation (CWPO) is a kind of Advanced Oxidation Processes (AOP)[10–13]. The efficiency of CWPO for the degradative removal of organic matters from wastewater is mainly based on high amounts of hydroxyl radicals (·OH) from the reaction of catalyst and H_2O_2. The generated hydroxyl radicals are highly reactive species and thus can unselectively react with organic matters and convert them into smaller molecular products, and even directly into CO_2 and H_2O[14,15]. The advantages of high efficiency and low intermediate pollutants make the CWPO process more attractive for treating complex organic wastewater[16,17]. The degradation efficiency of CWPO can be improved by enhancing the catalyst activity. Zero valent metals including nanoscale zero valent iron (nZVI)[18,19], zero valent aluminum (ZVAl)[20], and zero valent copper (ZVC)[12,21], could activate molecular oxygen to induce the generation of more powerful reactive oxygen species (ROS), such as superoxide radical anion ($\cdot O_2^-$) and hydroxyl radical (·OH). Copper is one of the major redox-active transition

Faculty of Environment and Life, Beijing University of Technology, Beijing 100124, China. ✉email: qinxia@bjut.edu.cn

	Advantages	Disadvantages
Coagulation and flocculation	Removing macromolecular colloidal organics effectively; low operation cost	Requires using more chemicals, leading to the generation of more sludge
Adsorption	Convenience, ease of operation, and simplicity of design; removing organic matter with molecular weight of 500–3000 da effectively	Macromolecular organic compounds are easy to block the pore structure of adsorbent; not suitable for high concentration wastewater
Membrane filtration	Removing organic matter, salt and pathogenic microorganisms in water effectively	Causing irreversible membrane fouling by pore narrowing and the formation of loose cake layer; the membrane concentrate should be treated further
Advanced oxidation processes	Removing all kinds of organic matter effectively without selectivity	High operating costs

Table 1. The methods of FA removal.

metal catalysts, but the application of Cu catalyst in CWPO was severely limited due to the instability of Cu^+. However, ZVC has a potential capacity to release Cu^+ through oxidation to activate H_2O_2 to generate ·OH thereby resulting in the degradation of organic contaminants[12,20].

Activated carbons have good performance in adsorption and catalysis[22]. Activated carbons can be produced through either physical or chemical activation. Physical activation involves pyrolysis of a carbonaceous precursor to produce a char follower by some activating agents such as carbon dioxide or steam. In the chemical activation, the precursor was pretreated with chemical activator (e.g. $ZnCl_2$, H_3PO_4, KOH and NaOH), and then thermal treated via pyrolysis to produce an activated carbon[23]. Williams[24] produced activated carbon via both physical and chemical activation with biomass waste flax fibre as precursor. The results showed that physical activation produced activated carbons with a nodular and pitted surface morphology whereas activated carbons produced through chemical activation had a smooth surface morphology. TEM analysis could identify mesoporous structures in the physically activated carbon and microporous structures in the chemically activated carbons. Sahira et al.[25] used different activating agents (KOH, H_2SO_4, $FeCl_3$, $MgCl_2$ and $CaCl_2$), and found out that the different activating agents have no significant effect on the nature of surface functional groups, with all showing similar oxygenated functional groups in FT-IR such as hydroxyl, carbonyl, carboxyl and lactones. Ahmed et al.[26,27] prepared activated carbon via two-stage activation using H_3PO_4 and KOH and the produced activated carbon possessed high surface area (692.3 and 1368 m^2/g) and pore volume (0.44 and 0.92 cm^3/g).

Chitosan (CS), the second most abundant biopolymer after cellulose in nature and derived from chitin of crab shells and fungus cell walls[28], has gradually attracted the attention of researchers[28–32] due to its non-toxicity and biocompatible, cost-effective nitrogen precursor, and environmentally friendly features. Hitherto, CS and its derivatives were used in different areas including flocculating agents, adsorbents, catalyst, thickeners, food preservation, and many others[33,34]. Recently, a variety of carbon materials has been developed from CS and used in different applications, thereby highlighting its great impact on chemistry and material science[35]. He et al. prepared activated carbon by surface modification with CS as nitrogen source during KOH activation process, displaying a remarkable CO_2 uptake achievement of 0.00583 mol/g[36]. In addition, CS contains abundant hydroxy and amine functional groups, which are responsible for its easy incorporation with the other materials[31]. CS can serve as a chelating agent for 3d metal ions such as Fe^{3+}, Cu^{2+} and Ni^{2+} because of its flexible structure and high chemical reactivity[32]. The CS-derived metal–carbon nanocomposites can serve as catalysts due to their textural properties, the presence of nitrogen species, and the uniform dispersion of metal nanoparticles[35]. Guo et al.[37] prepared the chitosan-supported iron (III) tetraphenylporphyrin. In their study, under reaction conditions of 418 K and 0.8 MPa, the cyclohexane oxidation catalyzed by chitosan-supported iron (III) tetraphenylporphyrin had 10.48% cyclohexane conversion and 79.20% cyclohexanone and cyclohexanol selectivity. Wang et al.[38] prepared the Cu–M@CS–SiO_2 degrading 1,1-dimethyl hydrazine (UDMH) wastewater. The COD removal of UDMH wastewater was 87.38% in half an hour.

Traditionally, the CWPO experimental conditions have been optimized by several single-factor or orthogonal experiments, in which the optimal conditions can be found only within the chosen experiment points. Additionally, these traditional methods also ignore the interaction among some parameters[37]. Plackett–Burman (PB)[39,40] design is a statistical method for screening the significant influence factors in multi-factors experiments. The statistical experiment design of the response surface method (RSM) can optimize the values of all the influence parameters including the interaction factors and provide an optimal prediction model for the experiments. RSM can even find the optimal target response point outside the set condition interval[41].

In this study, chitosan was used to produce stable chelates with copper ions and then the chitosan chelates was carbonated to provide well-distributed ZVC active sites[42]. The chitosan-activated carbon was used as both an adsorbent for adsorbing organic compounds to the reaction site and more importantly a carrier to support active metals of the catalyst. Additionally, carbon was used to reduce Cu^{2+} to Cu^0 during the pyrolysis, which makes the catalyst perform better in the CWPO. The purpose of this study was to evaluate the efficiency of FA removal in the CWPO process with ZVC/CTS-ACB as catalyst. The RSM coupled with PB was used to optimize the parameters of the CWPO experiment. The catalyst was prepared and the catalytic performance in CWPO was investigated in comparison with other degradation processes in removal of FA, TOC and colour number (CN).

Materials and methods

Materials. FA was purchased from Cool Chemical Technology Corporation (Beijing). The appearance color of the FA solution varies from dark yellow to light yellow depending on the concentration. Chitosan was supplied by Jinan Haidebei Marine Bioengineering, whose Deacetylation Degree ≥ 85%, Particle ≥ 40 Mesh and viscosity = 200 mpas. All other agents were of analytical grade and purchased from Beijing Chemical Plant. The pH

of the FA solution was adjusted by adding H_2SO_4 or NaOH. All the water used in the experiment was deionized water, from a Millipore-Q system with a resistance of 18.2 MΩ.

Preparation and characteristics of ZVC/CTS-ACB. The preparation of ZVC/CTS-ACB was carried out according to the following steps: (1) Preparation of chitosan gel: 7.25 g of $CuNO_4{\cdot}3H_2O$ was weighed and dissolved in 960 ml of deionized water, at the same time 0.1 g of citric acid was added, and then 30 g of chitosan was weighed and dispersed in a copper nitrate solution to form a suspension. 40 ml of acetic acid was added and stirred quickly and uniformly until a gel was formed. The gel was allowed to stand overnight to discharge air bubbles. (2) The gel was added dropwise to a 3.75 to 5 wt% sodium hydroxide solution using a syringe, then allowed to stand for 4–6 h. (3) After washing to neutral and drying at 60–100 °C for one night, the precursor was kept at 800–850 °C for 2–5 h in an inert gas tube furnace to complete its carbonization and become an activated carbon ball. (4) The activated carbon ball was rinsed several times in ethanol and deionized water, and then dried at 80 °C to remove moisture.

Experimental studies. The CWPO reaction was carried out in a reactor whose temperature can be controlled. The pH value of the water sample was adjusted by 0.5 M H_2SO_4 and 1 M NaOH solutions, and an appropriate amount of ZVC/CTS-ACB was added to the water sample. When the reaction temperature reached the set temperature, 30% of H_2O_2 was dropped into the reactor through the transfer pipe to make hydrogen oxide fully contact the catalyst to produce strong oxidizing free radicals[43], such as ·OH, $\cdot O_2$, etc. These free radicals can oxidize organics into small molecular organics and even H_2O and CO_2. Samples were taken every ten minutes from the reaction effluent under different conditions. MnO_2 was added to the sample to prevent the influence of excess H_2O_2 on the detection results, and then the sample was filtered through a 0.45 μm membrane for the subsequent results testing.

Analytical methods. The surface and profile morphology of the catalyst and the distribution of the supported metal crystals were observed using SEM (FEI Quanta 200). The active crystal phase composition of the catalyst was identified by XRD (D8 Advance type). The element composition was analyzed by the XPS. The chemical group was detected by the FT-IR (IRPrestige-21). Total copper ion in solution was quantified by the ICP. The pH value was measured using a pH meter (pHs-3C type). The total organic carbon (TOC) of the influent and effluent was analyzed using a total organic carbon analyzer (TOC-5000A, Shimadzu, Japan), and the mineralization rate (α, %) was calculated by Eq. (1).

$$\alpha = \frac{TOC_0 - TOC}{TOC_0} \times 100\%, \tag{1}$$

where TOC_0 is the initial concentration and TOC is the effluent concentration.

The absorbance of FA was measured at a wavelength of 254 nm using an Ultraviolet–Visible spectrophotometer (Hitachi U-3900). The removal rate (β, %) of the FA is calculated by Eq. (2).

$$\beta = \frac{UV_{254(0)} - UV_{254}}{UV_{254(0)}} \times 100\%. \tag{2}$$

The color number of FA can be calculated and analyzed by UV–Vis[44]. Since the visible region of the leachate spectrum showed no limited absorption maxima, the colour number (CN) defined by Eq. (3) was used to characterize the colour. CN relies on the measurement of the spectral absorption coefficient (SAC) in the visible range at wavelengths of 436, 525 and 620 nm. SAC is determined by the absorption value (Abs) divided by a cell of thickness x, which is shown in Eq. (4).

$$CN = \frac{SAC_{436}^2 + SAC_{525}^2 + SAC_{620}^2}{SAC_{436} + SAC_{525} + SAC_{620}}, \tag{3}$$

$$SAC_i = \frac{Abs_i}{x}. \tag{4}$$

The CN removal rate (γ, %) of FA is calculated by Eq. (5).

$$\gamma = \frac{CN_i - CN_0}{CN_i} \times 100\%. \tag{5}$$

Plackett–Burman and response surface methodology. The Design Expert Software (version 8.0) was used for experiment design and data analysis. Plackett–Burman (PB) coupled with central composite design response surface methodology (CCD-RSM) were used to evaluate and optimize the impact factors. Taking the removal rate of FA as the response target, two steps were used to optimize the experimental factors: Firstly, the PB experimental design was used to select the factors that significantly influenced the response, then CCD of RSM is used to find the optimum experimental conditions. During the experiment period, the CWPO was performed to degrade FA according to the designed conditions, the absorbance values of the FA samples before and after the reaction were measured at a wavelength of 254 nm, and the removal rate of the target fulvic acid was calculated by Eq. (2). After the experiment, the second-order response surface model equation was obtained and

Variable	X1:A	X2:B	X3:C	X4:D	X5:E	X6:F	X7:G	X8, X9, X10, X11 (H, I, J, K)
Factors	Temperature/°C	Initial volume/ml	Initial FA concentration/ mg/L	Time/min	H_2O_2/mmol	(ZVC/CTS-ACB)/g/L	Acidity	–
High level (+)	90	250	100	45	10	3	4	–
Low level (−)	60	500	200	90	20	5	7	–

Table 2. Factors of PB design experiment.

the optimal experimental conditions were determined by PB and CCD-RSM, and finally the optimal conditions were verified by conducting three repetitive tests.

Plackett–Burman experiment. The Plackett–Burman experimental design was proposed by Plackett and Burman in 1946. It was based on the principle of incompletely balanced plates. At most (N − 1) variables (N was generally a multiple of 4) could be studied by N experiments[45]. During the experiment, dummy variables are usually reserved as error analysis. Each variable has two levels, high and low, marked as (+) and (−), respectively.

The Plackett–Burman design of the CWPO experiment was shown in Table 2. The seven main factors of the FA degradation experiment were screened, plus four dummy variables. Each variable was determined at two levels (+) and (−), and a total of 12 experiments were conducted to determine the impact factors.

Response surface methodology. The Central Composite Design (CCD) developed by Box and Wilson is a commonly used response surface design method, with which an optimal fitted model can be obtained with minimum numbers of experiments. The second-order empirical model is generally used to characterize the response behavior of variables.

$$Y = \beta_0 + \sum_{i=1}^{k} \beta_i X_i + \sum_{i=1}^{j-1} \sum_{j=1}^{k} \beta_{ij} X_i X_j + \sum_{i=1}^{k} \beta_{ii} X_i^2,$$

where: Y represents the system response; β_0, β_i, β_{ii} are the offset term, linear offset and second-order offset coefficient, respectively; β_{ij} is the interaction coefficient; X_i is the horizontal value of each factor.

Comparative experiment of catalytic performance. In order to better understand the role of the catalyst (ZVC/CTS-ACB) in the CWPO process, the UV_{254}, TOC and CN removal efficiency of FA was investigated in various CWPO systems.

Results and discussion

Characterization of ZVC/CTS-ACB. The composition of the ZVC/CTS-ACB was characterized by X-ray diffraction (XRD) and X-ray photoelectron spectrometry (XPS). The diffraction peaks at 43.46°, 50.56° and 74.31° match well with the standard pattern of zero-valent copper (JCPDS 85-1326) (Fig. 1a)[46]. The crystalline grain size of Cu was calculated as 7.76 nm by the Williamson–Hall method. The Cu2p XPS spectrum (Fig. 1b) showed the peak of CuO at 943.3 eV as well as peaks of Cu^0 at 931.7 eV and 951.6 eV[46]. All results showed that zero-valent copper existed in the catalyst. The absorption bands for ZVC/CTS-ACB (Fig. 1c) are 925.8, 1099.4 and 3437.1 cm^{-1}, which correspond to C–O–C stretching, C=O bending and O–H stretching. All of these indicate the carboxyl groups on ZVC/CTS-ACB[47], which may facilitate electron transfer[48]. Furthermore, the scan electron microscopy (SEM) morphologies (Fig. 2) showed that the ZVC/CTS-ACB have porous network structure on the surface, and the cross-sectional view showed uniform distribution of copper microcrystalline particles in the interior. The BET results presented that the specific surface area, pore volume and pore size were 42.4 m^2/g, 0.98 cm^3/g and 1.9 nm, respectively.

Plackett–Burman experimental design results and analysis. The results of 12 runs of the FA removal experiments are shown in Table 3. The analysis of variance (ANOVA) results are shown in Table 4 with a list of significant differences of each factor impact.

As shown in Table 4, the Model's F-value of 51.46 proves the model is significant. There is only a very small chance (< 0.004) that the F-value of the model is the result of noise. In this case, A, G are significant model terms. Values greater than 0.1000 indicates the model terms are not significant. It could be concluded that only the temperature and acidity factors have significant effects on the target values among the seven factors considered. It has been reported that the higher the reaction temperature, the faster the reaction[49], and that pH can affect the chemical reaction rate and the production of free radicals[50]. Therefore, temperature and acidity were selected for the following central combination design.

CCD optimization design results and response surface analysis. The CCD was conducted for the Temperature and acidity selected by Plackett-Buiman with other non-critical factors fixed: Initial volume = 250 ml, Initial concentration = 100 mg/l, Time = 60 min, H_2O_2 = 20 mmol, (ZVC/CTS-ACB) = 3 g/l. The CWPO degradation FA experiment was performed according to the designed conditions, and the target response value was calculated.

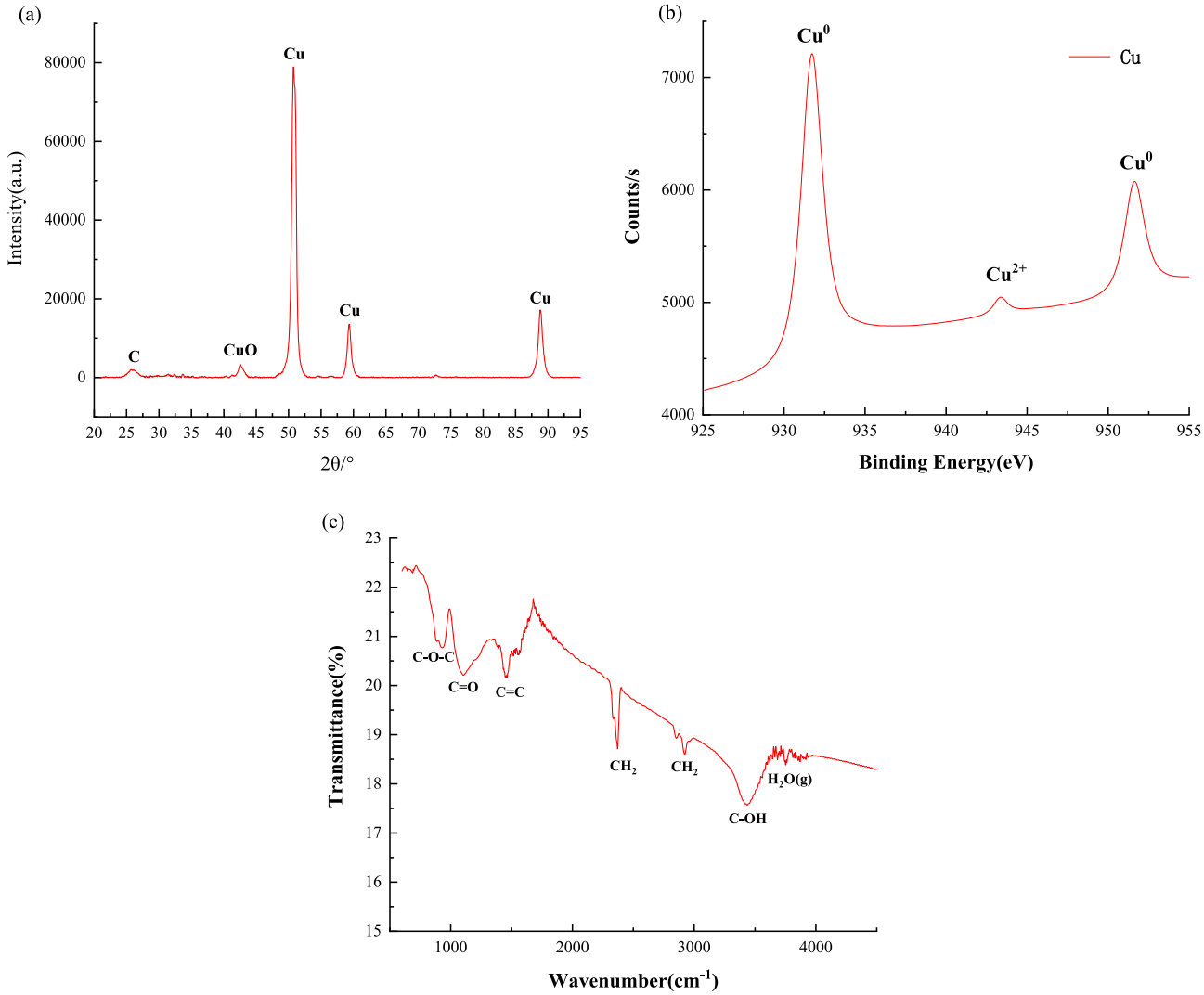

Figure 1. (**a**) XRD pattern of ZVC/CTS-ACB. (**b**) XPS of ZVC/CTS-ACB. (**c**) FT-IR of ZVC/CTS-ACB.

Model fitting and analysis of variance. Table 5 shows the conditions of 13 runs and the value of FA removal rates. Evaluation of data in this table provides a second-order polynomial to express the relationship between FA removal efficiency and the experimental parameters.

$$Y = 80.25 + 15.98A + 20.28B - 6.64A^2 - 25.70B^2,$$

where: Y is the target response value, i.e. the removal of the FA. A and B represent temperature and acidity, respectively.

Table 6 shows the results of the RSM model fitting in the form of an analysis of variance (ANOVA). According to the table, the high F-value (F-value = 29.21) and the very low probability values (P value < 0.0001) indicates the model obtained is highly significant. At the same time, the F-value of the missing term is 4.66, indicating that the missing term has no significant effect, so the established model can be referenced[51]. From the corresponding P-value, it was shown that among the tested variables, the B-acidity and A-temperature value had the greatest influence on the removal efficiency of FA, and the surface effect of factor B^2 on the FA removal effect is significant.

The correlation system R^2 is an important reference for the degree of fit. When R^2 tends to be unified, the fit of the empirical model of the actual data is better. Joglekar and Ma[52] suggested that for a good fit of the model, R^2 should be at least 0.80. The R^2 value of this model was 0.9359, indicating that the regression model fits well with the experiment.

RSM analysis. Figure 3 is a response surface graph and its contour plot from the multiple regression Eq. (3). It can be seen that the 3D response surface graph presents an inverted "U" shape, and a "red peak" appears at the center of the right side, meaning that the target optimal response value is obtained near here[53]. In the case of a fixed temperature, the target response value first increases and then tends to be gradual, and finally decreases slowly. On the other hand, if the acidity value is fixed, the target response value increases slowly and slightly with the increasing temperature. This also demonstrated that the degree of influence of acidity on the target FA

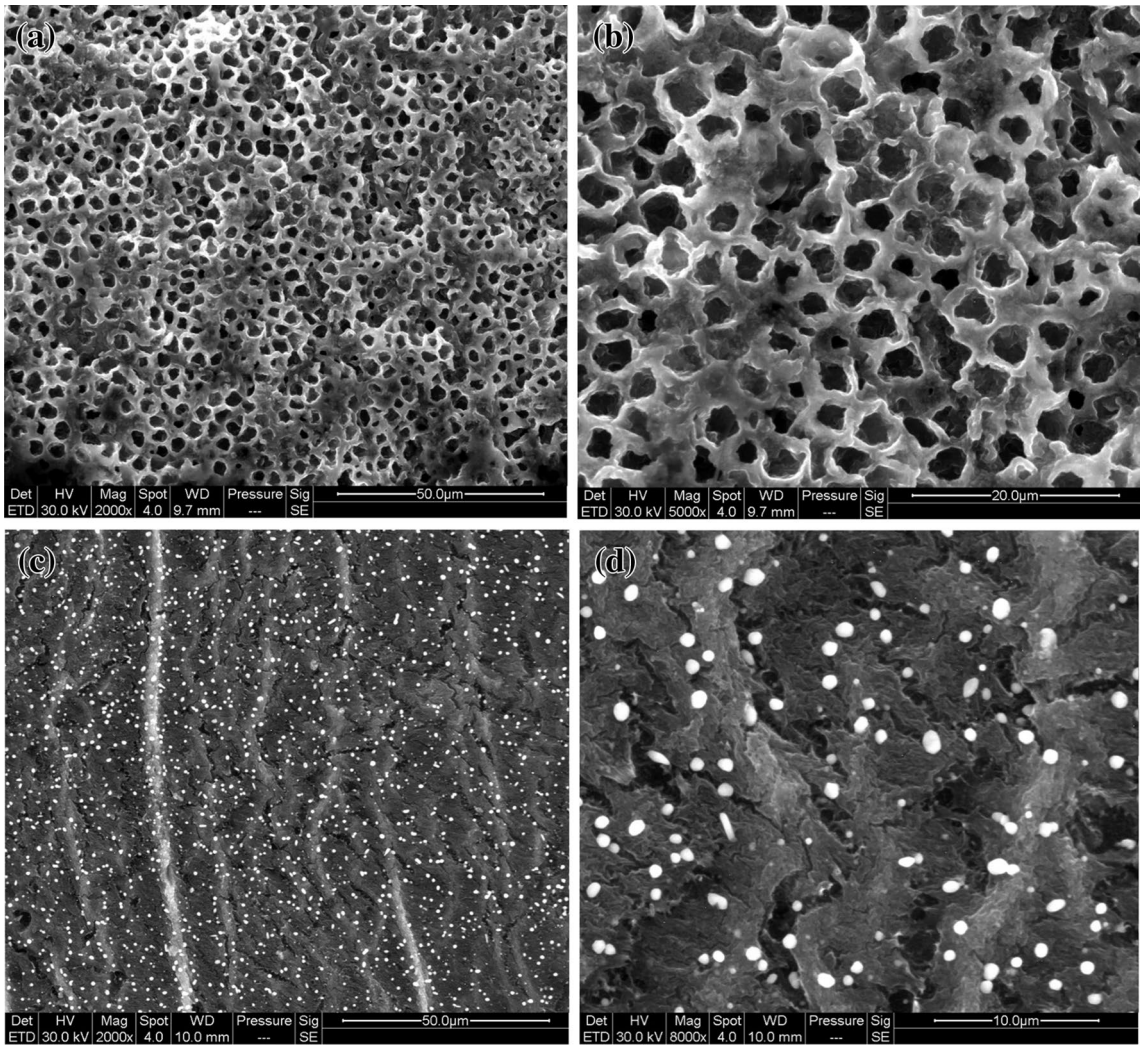

Figure 2. (**a**) SEM of outer surface is magnified 2000 times of ZVC/CTS-ACB. (**b**) SEM of outer surface is magnified 5000 times of ZVC/CTS-ACB. (**c**) SEM of inner cut surface is magnified 2000 times of ZVC/CTS-ACB. (**d**) SEM of inner cut surface is magnified 8000 times of ZVC/CTS-ACB.

Run	Factor: A	Factor: B	Factor: C	Factor: D	Factor: E	Factor: F	Factor: G	Response (%)
1	−	+	−	−	+	−	+	37.77
2	+	+	−	+	+	+	−	84.59
3	+	−	+	+	−	−	+	51.13
4	+	+	−	−	+	−	+	48.41
5	+	−	−	−	−	+	+	45.59
6	−	+	+	+	−	+	+	34.38
7	−	−	+	−	+	+	−	74.54
8	+	−	+	+	+	−	−	83.11
9	−	−	−	+	+	+	+	41.07
10	−	−	−	−	−	−	−	73.32
11	−	+	−	+	−	−	−	78.29
12	+	+	+	−	−	+	−	81.26

Table 3. PB design and response values.

Source	Mean square	F value	Value	Remarks
Model	525.97	51.46	0.0040	Significant
A	197.94	19.37	0.0218	Significant
B	1.66	0.16	0.7141	Not significant
C	6.21	0.61	0.4926	Not significant
D	8.32	0.81	0.4357	Not significant
E	2.18	0.21	0.6753	Not significant
F	8.32	0.81	0.4335	Not significant
G	338.98	37.13	0.0041	Significant

Table 4. ANOVA results.

Run	1	2	3	4	5	6	7	8	9	10	11	12	13
Factor A: temperature (°C)	90	90	70	50	70	70	98	42	70	70	70	70	50
Factor B: acidity	5.0	1.0	3.0	1.4	1.2	5.8	1.2	5.8	3.0	3.0	3.0	3.0	5.0
Response: removal rate of FA (%)	80.78	44.03	84.78	34.89	30.44	62.99	91.80	41.45	80.56	74.94	84.78	80.80	46.60

Table 5. CCD experimental design table.

Source	Sum of squares	Df	Mean square	F value	P-value	
Model	5405.22	4	1351.31	29.21	< 0.0001	Significant
A-temperature	2029.59	1	2029.59	43.87	0.0002	
B-acidity	2208.68	1	2208.68	47.74	0.0001	
A^2	311.26	1	311.26	6.73	0.0319	
B^2	2679.40	1	2679.40	57.92	< 0.0001	
Residual	370.11	8	46.26			
Lack of fit	304.72	4	76.18	4.66	0.0826	Not significant
R-squared	0.9359					
Adj R-squared	0.9039					

Table 6. ANOVA for the regression quadratic model of CCD design.

removal was greater than temperature. The shape of the contour plot indicates the nature and extent of the interaction. The regular elliptical nature of the contour plot shows significant interactions, while the near-circular nature of the contour plots shows less prominent or negligible interactions[53]. It can be seen from the contour plot in Fig. 3 that there is no strong interaction between the influencing factors A and B here, which is consistent with the results obtained by the ANOVA above (Table 6). From the contour plot, the optimal acid of the model could be obtained in the acid pH range of 3 to 5, whereas the optimal temperature could not be found, it might be over 90 °C, so the model did need further optimization.

Optimization of influencing factors. The main purpose of the optimization was to determine the optimal parameter values for maximizing the FA removal. Therefore, the maximum removal of FA was selected as the target value. Since the optimal temperature may emerge over 90 °C, the temperature range was enlarged from 60–90 to 60–130 °C. Then the optimum values were obtained, as shown in Fig. 4, whereby two optimization schemes were also obtained in Table 7. Since the conditions of the two schemes were very close, and the expected target values are not different from each other, the temperature and acidity were finally selected as 94 °C and pH 3.8 respectively for the convenience of the experimental conditions setting.

Figure 5 is the optimized 3D surface graph and contour plots. Compared with Fig. 3, a mountain shape 3D surface graph was obtained and it was obvious that the maximum removal of FA (93.8633%) was at the peak of the mountain.

Results verification. To confirm whether the model is sufficient to predict the maximum FA removal efficiency, three repetitive tests were performed under the optimal operating condition as shown in Table 8. The average maximum FA removal efficiency produced by three replicate experiments was 93.02%, while the RSM optimal target response was 93.86%. The good agreement between the predicted results and the experimental

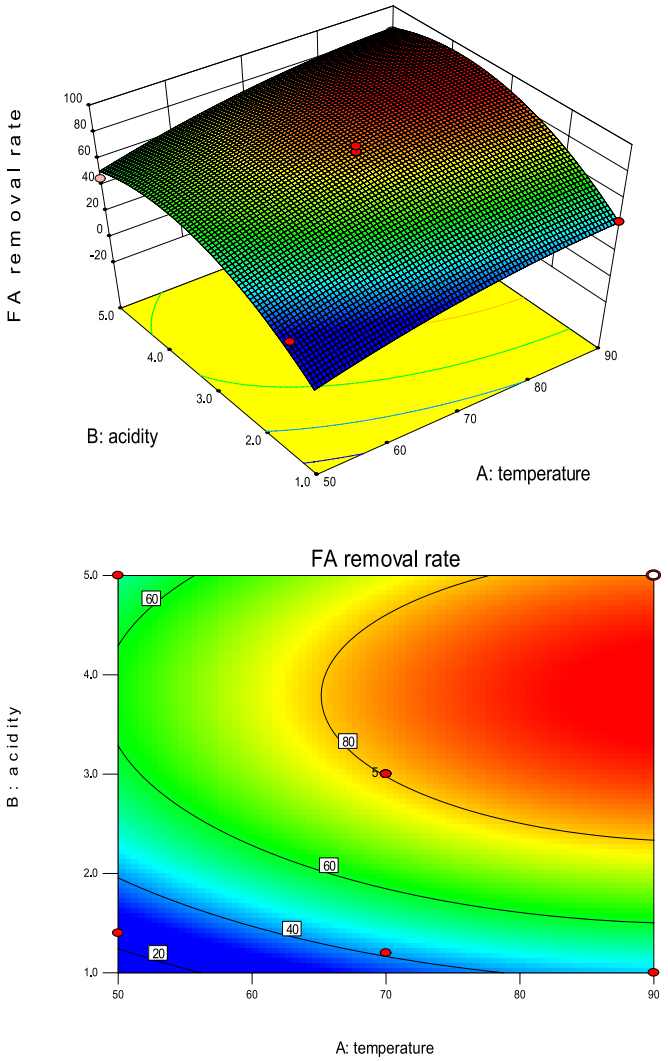

Figure 3. 3D response surface graph and contour plot.

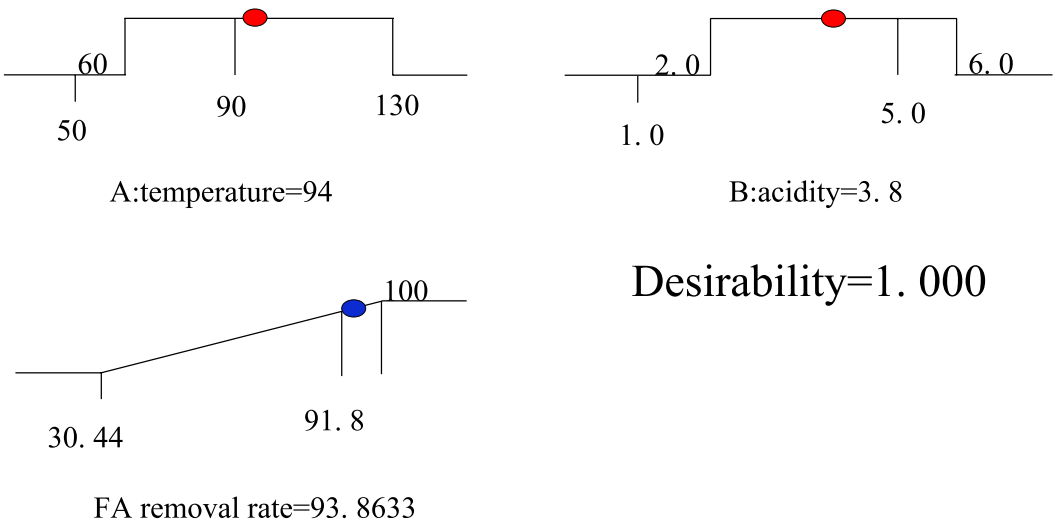

Figure 4. Desirable slope for numerical optimization of the CWPO conditions.

Solution	Temperature	Acidity	FA removal rate (%)	Desirability
1	94.07	3.8	93.8643	1.000
2	93.99	3.8	93.8622	1.000
Prediction	94	3.8	93.8633	1.000

Table 7. RSM system optimized solution.

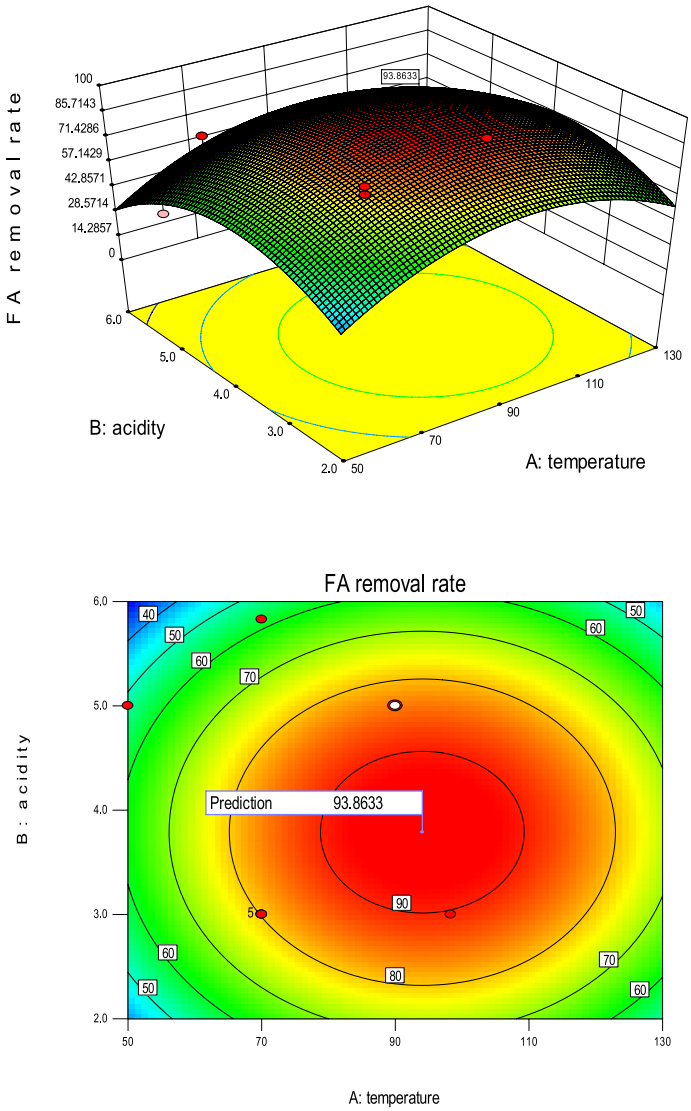

Figure 5. Optimized 3D surface graph and contour plots.

Parameter	Y (removal efficiency, %)		
Practice			
Times	1	2	3
Single	92.45	92.82	93.78
Average	93.02		
Prediction	93.86		

Table 8. Optimum value of the process parameter for maximum efficiency.

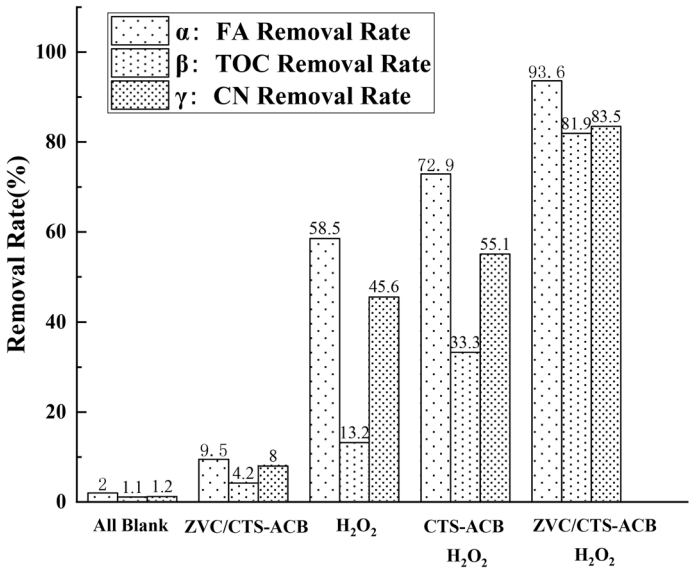

Figure 6. Catalyst and oxidant controlled trials (FA = 100 mg/l, temperature = 94 °C, time = 90 min, pH 3.8, CTS-ACB and ZVC/CTS-ACB = 4 g/l, H_2O_2 = 20 mmol).

results verifies the validity of the model and confirms that CCD-RSM is a powerful tool for optimizing the experimental factors.

Removal efficiency under different systems and the stability of ZVC/CTS-ACB. The removal rates of FA, TOC, and CN expressed by α, β, and γ respectively were shown in Fig. 6. It can be seen from the figure that the addition of oxidant H_2O_2 is crucial. The experimental groups with H_2O_2 added had better removal rates of FA, TOC and CN compared to those without H_2O_2. Among the latter three groups, the groups with catalyst achieved a higher removal rate than the group without catalyst. The removal rates of the three indicators had increased, especially the removal rate of TOC had improved significantly, from 13.2 to 81.9%, which indicates that the addition of ZVC could greatly increase the mineralization rate of FA in the CWPO reaction. Under the same condition, the mineralization rate was nearly 2.5 times higher than that of the experimental group without ZVC. ZVC also has obvious effects on FA degradation and color removal. All the results show that the ZVC/CTS-ACB catalyst prepared in this research has high catalytic activity in FA removal and organic compound mineralization.

The possible degradation mechanism might be: the reaction starts with the Cu^0 and H_2O_2, producing Cu^+ and OH^-, Cu^+ reacts with H_2O_2 producing ·OH and Cu^{2+}. The generated ·OH could mineralize FA into small molecules, even to CO_2 and H_2O.

The stability of ZVC/CTS-ACB was investigated through FA degradation repeating experiments in which the catalyst was repeated five times. The FA removal decreased from 94.78 to 90.05% in five runs. The ICP analysis of the effluent in the first run and fifth run showed that, the leaching concentrations of Cu ion were 0 mg/l and 0.08 mg/l respectively, which demonstrate the recyclability and stability of ZVC/CTS-ACB.

Conclusion

This study demonstrates the applicability of the prepared ZVC/CTS-ACB to the degradation of FA in CWPO. The statistical tools Plackett–Buiman and central composite design coupled with the response surface model were used to analyze the experimental data and predict the optimal target response value. Under the optimal conditions given by the system, the experiment was repeated three times. The average removal rate of FA was 93.02%, which was very close to the predicted target response value of 93.86%, indicating that the model was established accurately. The experiment results confirm that the PB experiment and the CCD-RSM are suitable for optimizing the operating conditions in a multi-factor operating environment to obtain the maximum FA degradation rate. The comparison experimental results showed that the catalyst and oxidant were essential factors in the CWPO reaction. The ZVC/CTS-ACB catalyst could greatly increase the mineralization rate of FA. The TOC removal rate of 81.9% indicated that most FA were directly mineralized into CO_2 and H_2O during the CWPO process, in which ZVC/CTS-ACB showed the high catalytic activity. The low leaching rate of copper ion also showed that the catalyst had good stability. Further study will be conducted on the catalytic mechanism of ZVC/CTS-ACS to FA removal and application of the catalyst in leachate treatment with CWPO.

Received: 21 December 2020; Accepted: 7 June 2021
Published online: 07 July 2021

References

1. Iskander, S. M. *et al.* A review of landfill leachate induced ultraviolet quenching substances: Sources, characteristics, and treatment. *Water Res.* **145**, 297–311 (2018).
2. Jones, M. N. & Bryan, N. D. Colloidal properties of humic substances. *Adv. Colloid Interface Sci.* **78**(1), 1–48 (1998).
3. Tang, W. *et al.* Impact of humic/fulvic acid on the removal of heavy metals from aqueous solutions using nanomaterials: A review. *Sci. Total Environ.* **468–469**, 1014–1027 (2014).
4. Sillanpaa, M. *et al.* Removal of natural organic matter in drinking water treatment by coagulation: A comprehensive review. *Chemosphere* **190**, 54 (2018).
5. Wang, J., Zhou, Y., Li, A. & Xu, L. Adsorption of humic acid by bi-functional resin JN-10 and the effect of alkali-earth metal ions on the adsorption. *J. Hazard. Mater.* **176**, 1018–1026 (2010).
6. Wang, S. *et al.* Chitosan hydrogel beads for fulvic acid adsorption: Behaviors and mechanisms. *Chem. Eng. J.* **142**, 239–247 (2008).
7. Zhao, L. *et al.* Adsorption of humic acid from aqueous solution onto irradiation-crosslinked carboxymethylchitosan. *Biores. Technol.* **99**, 1911–1917 (2008).
8. Zhang, J. *et al.* Simultaneous removal of humic acid/fulvic acid and lead from landfill leachate using magnetic graphene oxide. *Appl. Surf. Sci.* **370**, 335–350 (2016).
9. Matilainen, A. *et al.* An overview of the methods used in the characterisation of natural organic matter (NOM) in relation to drinking water treatment. *Chemosphere* **83**(11), 1431–1442 (2011).
10. Eftaxias, A., Font, J., Fortuny, A., Fabregat, A. & Stüber, F. Catalytic wet air oxidation of phenol over active carbon catalyst: Global kinetic modelling using simulated annealing. *Appl. Catal. B* **67**, 12–23 (2006).
11. Milone, C. *et al.* Catalytic wet air oxidation of p-coumaric acid over carbon nanotubes and activated carbon. *Ind. Eng. Chem. Res.* **50**, 9043–9053 (2011).
12. Wen, G. *et al.* Oxidative degradation of organic pollutants in aqueous solution using zero valent copper under aerobic atmosphere condition. *J. Hazard. Mater.* **275**, 193–199 (2014).
13. Zhou, P. *et al.* Activation of hydrogen peroxide during the corrosion of nanoscale zero valent copper in acidic solution. *J. Mol. Catal. A Chem.* **424**, 115–120 (2016).
14. Abecassis-Wolfovich, M., Landau, M. V., Brenner, A. & Herskowitz, M. Catalytic wet oxidation of phenol with Mn–Ce-based oxide catalysts: Impact of reactive adsorption on TOC removal. *Ind. Eng. Chem. Res.* **43**, 5089–5097 (2004).
15. An, W., Zhang, Q., Ma, Y. & Chuang, K. T. Pd-based catalysts for catalytic wet oxidation of combined Kraft pulp mill effluents in a trickle bed reactor. *Catal. Today* **64**, 289–296 (2001).
16. Poznyak, T., Bautista, G. L., Chaírez, I., Córdova, R. I. & Ríos, L. E. Decomposition of toxic pollutants in landfill leachate by ozone after coagulation treatment. *J. Hazard. Mater.* **152**, 1108–1114 (2008).
17. Rivas, J., Beltrán, F., Carvalho, M. D. F. & Alvarez, P. Oxone-promoted wet air oxidation of landfill leachates. *Ind. Eng. Chem. Res.* **44**, 749 (2005).
18. Oh, S. Y. & Shin, D. S. Degradation of spent caustic by Fenton and persulfate oxidation with zero-valent iron. *J. Chem. Technol. Biotechnol.* **88**, 145 (2012).
19. Keenan, C. R. & Sedlak, D. L. Factors affecting the yield of oxidants from the reaction of nanoparticulate zero-valent iron and oxygen. *Environ. Sci. Technol.* **42**, 5377 (2008).
20. Liu, W. *et al.* Oxidative removal of bisphenol A using zero valent aluminum–acid system. *Water Res.* **45**(4), 1872–1878 (2011).
21. Zhou, P. *et al.* Activation of hydrogen peroxide during the corrosion of nanoscale zero valent copper in acidic solution. *J. Mol. Catal. A: Chem.* **424**, 115–120 (2016).
22. Rodríguez-Reinoso, F. The role of carbon materials in heterogeneous catalysis. *Carbon* **36**(3), 159–175 (1998).
23. Ahmadpour, A. & Do, D. D. The preparation of active carbons from coal by chemical and physical activation. *Carbon* **34**(4), 471–479 (1996).
24. Williams, P. T. & Reed, A. R. Development of activated carbon pore structure via physical and chemical activation of biomass fibre waste. *Biomass Bioenergy* **30**(2), 144–152 (2006).
25. Sahira, J., Mandira, A., Prasad, P. B. & Ram, P. R. Effects of Activating Agents on the Activated Carbons Prepared from Lapsi Seed Stone. *Res. J. Chem. Sci.* **3**, 19 (2013).
26. Osman, A. I. *et al.* Upcycling brewer's spent grain waste into activated carbon and carbon nanotubes via two-stage activation for energy and other applications. *J. Chem. Technol. Biotechnol.* **95**, 183 (2019).
27. Osman, A. I. *et al.* The production and application of carbon nanomaterials from high alkali silicate herbaceous biomass. *Sci. Rep.* https://doi.org/10.1038/s41598-020-59481-7 (2020).
28. Chen, X. *et al.* Surface construction of nitrogen-doped chitosan-derived carbon nanosheets with hierarchically porous structure for enhanced sulfacetamide degradation via peroxymonosulfate activation: Maneuverable porosity and active sites. *Chem. Eng. J.* **382**, 122908 (2020).
29. Sjab, C. *et al.* Preparation and pore-forming mechanism of hydrogen bond and ionic bond double-driven chitosan-based mesoporous carbon. *Int. J. Biol. Macromol.* **179**, 519–531 (2021).
30. Liu, Y. *et al.* Chitosan modified nitrogen-doped porous carbon composite as a highly-efficient adsorbent for phenolic pollutants removal. *Colloids Surf. A Physicochem. Eng. Asp.* **610**, 125728 (2020).
31. An, A. *et al.* Facile synthesis of graphitic carbon nitride/chitosan/Au nanocomposite: A catalyst for electrochemical hydrogen evolution. *Int. J. Biol. Macromol.* **164**, 3012–3024 (2020).
32. Zhao, Y. *et al.* Self-assembled gels of Fe-chitosan/montmorillonite nanosheets: Dye degradation by the synergistic effect of adsorption and photo-Fenton reaction. *Chem. Eng. J.* **379**, 122322 (2020).
33. Kadib, A. E., Bousmina, M. & Brunel, D. Recent progress in chitosan bio-based soft nanomaterials. *J. Nanosci. Nanotechnol.* **14**(1), 308–331 (2014).
34. Elkadib, A. Chitosan as a sustainable organocatalyst: A concise overview. *Chemsuschem* **8**, 217 (2015).
35. Nha, B. *et al.* Chitosan as a sustainable precursor for nitrogen-containing carbon nanomaterials: synthesis and uses. *Mater. Today Sustain.* **10**, 100053 (2020).
36. Song, H. A. *et al.* Facile preparation of N-doped activated carbon produced from rice husk for CO_2 capture. *J. Colloid Interface Sci.* **582**, 90–101 (2021).
37. Guo, C. C. *et al.* Catalysis of chitosan-supported iron tetraphenylporphyrin for aerobic oxidation of cyclohexane in absence of reductants and solvents. *Appl. Catal. A* **247**(2), 261–267 (2003).
38. Wang, J. *et al.* Chitosan–silica nanoparticles catalyst (M@CS–SiO2) for the degradation of 1,1-dimethylhydrazine. *Res. Chem. Intermediat.* **45**, 1721 (2018).
39. Casey, T. J. & Chua, K. H. The design of optimum multifactorial experiments. *Biometrika* **33**, 305–325 (1946).
40. Weuster-Botz, D. Experimental design for fermentation media development: Statistical design or global random search. *J. Biosci. Bioeng.* **90**, 473–483 (2000).

41. Amiri, A. & Sabour, M. R. Multi-response optimization of Fenton process for applicability assessment in landfill leachate treatment. *Waste Manage.* **34**, 2528–2536 (2014).
42. Jian, Q. *et al.* The preparation and characterization of chitosan rods modified with Fe^{3+} by a chelation mechanism. *Carbohyd. Res.* **346**(6), 822–827 (2011).
43. Luan, M. *et al.* A review: Wet oxidation and catalytic wet oxidation of industrial wastewater. *Recent Patents Chem. Eng.* **6**, 79 (2013).
44. Tizaoui, C., Bouselmi, L., Mansouri, L. & Ghrabi, A. Landfill leachate treatment with ozone and ozone/hydrogen peroxide systems. *J. Hazard. Mater.* **140**, 316–324 (2007).
45. Plackett, R. L. & Burman, J. P. The design of optimum multifactorial experiments. *Biometrika* **33**, 305–325 (1946).
46. Zhang, Y., Fan, J., Yang, B., Huang, W. & Ma, L. Copper–catalyzed activation of molecular oxygen for oxidative destruction of acetaminophen: The mechanism and superoxide-mediated cycling of copper species. *Chemosphere* **166**, 89–95 (2017).
47. Wan Ngah, W. S., Teong, L. C. & Hanafiah, M. A. K. M. Adsorption of dyes and heavy metal ions by chitosan composites: A review. *Carbohyd. Polym.* **83**(4), 1446–1456 (2011).
48. Quintanilla, A., Fraile, A. F., Casas, J. A. & Rodrıguez, J. J. Phenol oxidation by a sequential CWPO–CWAO treatment with a Fe/AC catalyst. *J. Hazard. Mater.* **146**, 582–588 (2007).
49. Li, N., Descorme, C. & Besson, M. Catalytic wet air oxidation of chloropHenols over supported ruthenium catalysts. *J. Hazard. Mater.* **146**(3), 602–609 (2007).
50. Rahim Pouran, S., Abdul Raman, A. A. & Wan Daud, W. M. A. Review on the application of modified iron oxides as heterogeneous catalysts in Fenton reactions. *J. Clean. Prod.* **64**, 24–35 (2014).
51. Abdulredha, M. M., Hussain, S. A. & Abdullah, L. C. Optimization of the demulsification of water in oil emulsion via non-ionic surfactant by the response surface methods. *J. Pet. Sci. Eng.* **184**, 106463 (2020).
52. Fu, J., Ji, M., Zhao, Y. & Wang, L. Kinetics of aqueous photocatalytic oxidation of fulvic acids in a photocatalysis–ultrafiltration reactor (PUR). *Sep. Purif. Technol.* **50**, 107–113 (2006).
53. Kim, S. Application of response surface method as an experimental design to optimize coagulation–flocculation process for pre-treating paper wastewater. *J. Ind. Eng. Chem.* **38**, 93–102 (2016).

Author contributions

C.S. designed the experiment, and wrote the main manuscript text, Y.L. added some experiments and wrote a small part of the article. C.G. and J.C. did a part of experiment. X.Q. and K.W.S.-H. reviewed the manuscript.

Funding

The fund of conducting researches and preparation of the article was supported by the National Natural Science Foundation of China, China. (No. 51478009).

Competing interests

The authors declare no competing interests.

Additional information

Correspondence and requests for materials should be addressed to X.Q.

Reprints and permissions information is available at www.nature.com/reprints.

Publisher's note Springer Nature remains neutral with regard to jurisdictional claims in published maps and institutional affiliations.

Open Access This article is licensed under a Creative Commons Attribution 4.0 International License, which permits use, sharing, adaptation, distribution and reproduction in any medium or format, as long as you give appropriate credit to the original author(s) and the source, provide a link to the Creative Commons licence, and indicate if changes were made. The images or other third party material in this article are included in the article's Creative Commons licence, unless indicated otherwise in a credit line to the material. If material is not included in the article's Creative Commons licence and your intended use is not permitted by statutory regulation or exceeds the permitted use, you will need to obtain permission directly from the copyright holder. To view a copy of this licence, visit http://creativecommons.org/licenses/by/4.0/.

© The Author(s) 2021